GAMMA CURVE DETERMINATION FOR EACH INDIVIDUAL PIXEL ON HIGH-RESOLUTION FLAT PANEL DISPLAY

*Mina Kim**, *Won Hee Lee**, *Se Yun Kim***, *Hee Joon Kim***, *Hoisik Moon***, *and Jong Beom Ra**

*Department of Electrical Engineering, KAIST, Daejeon, Republic of Korea
{makim, whlee}@issserver.kaist.ac.kr, jbra@kaist.ac.kr
**Samsung Display Co., Ltd., Asan-City, Republic of Korea
{seyun1.kim, heejoon03.kim, hoisik.moon}@samsung.com

ABSTRACT

This paper presents an automated system to determine gamma curves of each individual pixel on a high-resolution flat panel display. The system consists of a panel and its aligned area scan camera located at a fixed position. To localize a panel pixel position in an image captured from the aligned camera, a mapping function estimation scheme is proposed between the panel and the camera coordinates. The mapping function is modeled by combining both 2-D perspective transform and lens distortion and is estimated via feature-based registration. Intensity values of individual panel pixel are then measured for sampled gray-levels. To alleviate intensity interferences from neighboring pixels, we propose to use evenly spaced dot images as panel input. By using the measured intensity values of each panel pixel, gamma curves are determined to examine the characteristics of defects on the panel, if any. Experimental results show the relevance of the proposed method.

Index Terms— Defect inspection, machine vision, high-resolution flat panel display, gamma curve determination

1. INTRODUCTION

The size of flat panel display (FPD) has steadily increased for many years in most of its applications such as TV, monitor, public display, and so on. Accordingly, ultra high definition (UHD) TVs of 4K or 8K resolution have been introduced recently. As FPD becomes larger with higher resolution, it is hard and time consuming for a human to inspect defects on it. Hence, automated optical inspection (AOI) systems have been developed for FPD, based on machine vision technology [1-5]. Most AOI systems were, however, mainly focused on the detection of defect positions.

In this paper, we propose an automated system to obtain gamma curves of each individual pixel on high-resolution FPD so that we can detect defect pixels and examine their characteristics.

A gamma curve of a pixel on a large high-resolution panel may be determined from its panel intensities measured by a digital camera. There are two kinds of digital cameras available for this purpose, namely, a line scan camera and an area camera. A line scan camera offers much higher resolution even compared to the UHD panel resolution so that it can be used in many machine vision applications including AOI. Nonetheless, line scan camera imaging requires not only the mechanical movement of an object or a camera and also precise synchronization of the movement and the camera acquisition.

Meanwhile, an area scan camera can put a whole panel in a single picture, but the resolution of captured image is not enough for examining the pixel intensity on a high-resolution panel due to blurring in the image acquisition system. For example, a 4K UHD TV includes 3840 x 2160 pixels, or 8 megapixels. In contrast, a recently announced high-resolution area scan camera has only 29 megapixel resolution, which is less than 4 times more than that of 4K UHD panel. Hence, even with a high-resolution area camera, the intensity of an individual panel pixel is hard to be accurately measured.

In the proposed method, we first estimate a mapping function between the panel coordinates and the camera coordinates. By using a checkerboard pattern image as a panel input, the estimation is performed via feature-based registration. Next, uniform images are displayed on the panel, for different input gray-levels, and captured by an area scan CCD camera. These images are then transformed and undistorted by applying the estimated mapping function to determine gamma curves of each individual panel pixel. For this determination, we propose a method to accurately measure panel pixel intensities from the captured images even though the images are blurred and under-sampled.

The paper is organized as follows: Section 2 describes details of the proposed methods for the estimation of mapping function, the measurement of individual panel pixel intensity values, and the determination of gamma curves. In Section 3, experimental results are given. Finally a conclusion is made in Section 4.

2. METHOD

The proposed automated vision system intends to obtain gamma curves of respective panel pixels. A gamma curve is defined as measured panel pixel intensities along the input gray-level axis. To obtain the intensity of a panel

978-0-9928626-3-3/15/$31.00 ©2015 IEEE

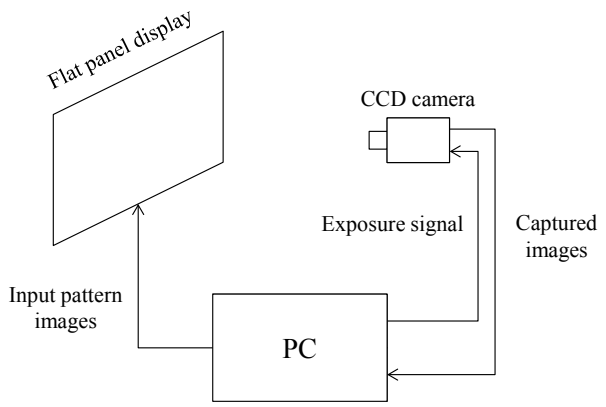

Fig. 1. Overall system configuration

pixel for a given gray-level, the location of a panel pixel has to be accurately determined in a captured panel image that is acquired using the system illustrated in Figure 1. This location determination can be done by estimating a mapping function that defines the transformation relationship between the panel coordinates and the camera coordinates. Note that the mapping function needs to be estimated only once in the entire process, because the panel and camera positions are fixed.

Once the location of a panel pixel is determined in the captured image, the intensity values of each panel pixel can be measured according to the sampled input gray-levels. The gamma curve is then determined via the interpolation of the measured intensity values along the input gray-level axis. Details are described in the following subsections.

2.1. Mapping function estimation

The discrepancy between the panel and camera coordinate systems comes mainly from the alignment error and the camera optical distortion. Therefore, in the proposed method, we parameterize the mapping function based on the models of 2-D perspective transform and lens distortion.

To determine a mapping function, we display a checkerboard pattern image on the panel and capture the displayed image by using a CCD camera. In the captured image, we detect the positions of corner points with subpixel accuracy. By minimizing the distances between the detected corner points and the corresponding original corner points in the panel coordinates, the parameters of mapping function are optimized via nonlinear least squares.

2.1.1. Model

Mapping function is parameterized by modeling both 2-D perspective transform and lens distortion. The 2-D perspective transform represents the relationship between the panel plane and the camera sensor plane, and can be written as

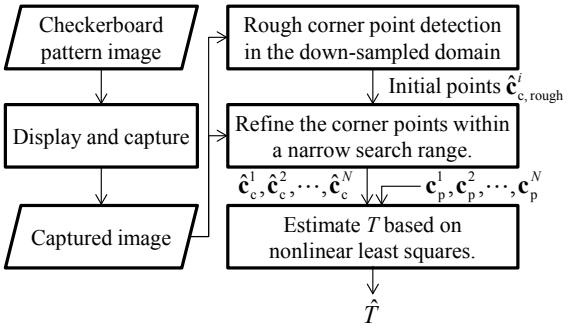

Fig. 2. Block diagram for mapping function estimation

$$\begin{pmatrix}\mathbf{x}_{\mathrm{p}}\\1\end{pmatrix}=\frac{\begin{pmatrix}a & b & c\\ d & e & f\\ g & h & 1\end{pmatrix}\begin{pmatrix}\mathbf{x}_{\mathrm{c}}\\1\end{pmatrix}}{\begin{pmatrix}g & h & 1\end{pmatrix}\begin{pmatrix}\mathbf{x}_{\mathrm{c}}\\1\end{pmatrix}}, \tag{1}$$

where $\mathbf{x}_{\mathrm{p}}$ and $\mathbf{x}_{\mathrm{c}}$ denote matching positions in the panel coordinates and the camera coordinates, respectively, by assuming no distortion. Here, a to h denote 8 parameters of the 2-D perspective transform.

Lens distortion has been widely treated in the camera calibration problem. The Plumb Bob model [6] is generally used as a lens distortion model. By dividing lens distortion into radial distortion and tangential distortion, this model is defined as

$$\begin{aligned}\mathbf{x}_{\mathrm{c}}-\mathbf{cc}_{\mathrm{c}}=&(1+k_1r_{\mathrm{u}}^2+k_2r_{\mathrm{u}}^4+k_3r_{\mathrm{u}}^6)\begin{bmatrix}x\\y\end{bmatrix}\\&+\begin{bmatrix}2k_4xy+k_5(r_{\mathrm{u}}^2+2x^2)\\k_4(r_{\mathrm{u}}^2+2y^2)+2k_5xy\end{bmatrix},\end{aligned} \tag{2}$$

where

$$\mathbf{x}_{\mathrm{c,ud}}-\mathbf{cc}_{\mathrm{c}}=\begin{pmatrix}x\\y\end{pmatrix} \tag{3}$$

and

$$r_{\mathrm{u}}=\sqrt{x^2+y^2}\ , \tag{4}$$

and $\mathbf{x}_{\mathrm{c}}$ denotes a position with lens distortion. Here, $\mathbf{cc}_{\mathrm{c}}$ denotes the camera center in the camera coordinates, and $\mathbf{x}_{\mathrm{c,ud}}$ denotes the undistorted position of $\mathbf{x}_{\mathrm{c}}$. As in (2), lens distortion can be modeled with 5 parameters, namely, k_1, k_2, and k_3 for radial distortion and k_4 and k_5 for tangential distortion.

The mapping function is thereby defined with thirteen parameters in total to describe both 2-D perspective transform and lens distortion simultaneously.

2.1.2. Corner point detection

Since a checkerboard pattern image is used as a panel input image, exact positions of corner points of the pattern in the panel coordinates, $\mathbf{c}^i_{\mathrm{p}}$, $i = 1, \ldots, n$, where n is the

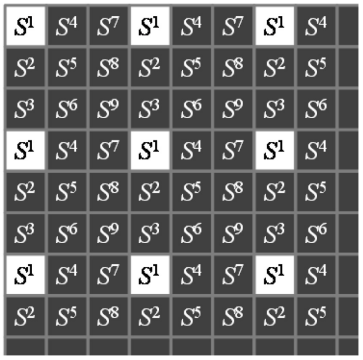

Fig. 3. An evenly spaced dot image for $m = 3$

number of corners to be matched, are already known. In order to efficiently detect corner positions in the camera coordinates from a captured pattern image, we propose a two-step approach.

In the first step, four outer corner points of the panel are determined in the ten times down-scaled captured image, via simple thresholding. A perspective transform is then approximately estimated by matching the four corner points to those in the panel coordinates. By using the estimated transform, $\mathbf{c}_{\mathrm{p}}^{i}$ are transformed into the down-scaled captured image domain. Rough corner positions are then determined around the transformed $\mathbf{c}_{\mathrm{p}}^{i}$, respectively, by using a corner detector that is described below.

In the second step, the detected positions are refined in the original size image using the same corner detector as in the first step, but with a smaller search range. We can thereby avoid a time consuming full search procedure in a large size image and reduce the possibility of outlier detection due to panel defects or camera noise in the captured image.

In both steps above, to determine corner points with sub-pixel accuracy, we adopt the Förstner corner detector [7,8]. The detector determines a corner point as an intersection of tangent lines of edges, which are defined by using image gradient vector, respectively. Here, the intersection is found as a least squares solution with gradient magnitude weights.

2.1.3. Estimation

According to Section 2.1.1, mapping function T is defined by using thirteen parameters. Using matching pairs of the positions of corners, $\left(\mathbf{c}_{\mathrm{p}}^{i}, \mathbf{c}_{\mathrm{c}}^{i}\right)$, T can be estimated via the optimization in a least squares sense. Namely,

$$\hat{T} = \arg\min_{T} \sum_{i=1}^{n} \left\| \mathbf{c}_{\mathrm{p}}^{i} - T^{-1}(\hat{\mathbf{c}}_{\mathrm{c}}^{i}) \right\|^2 . \qquad (5)$$

As T is a nonlinear function, Levenberg-Marquardt algorithm [9-11] is used as a nonlinear optimizer.

2.2. Panel pixel intensity measurement

Since the image acquisition system causes pixel blur in a captured image, to measure the intensity of individual panel pixel accurately, we need to avoid any interference from neighboring pixels.

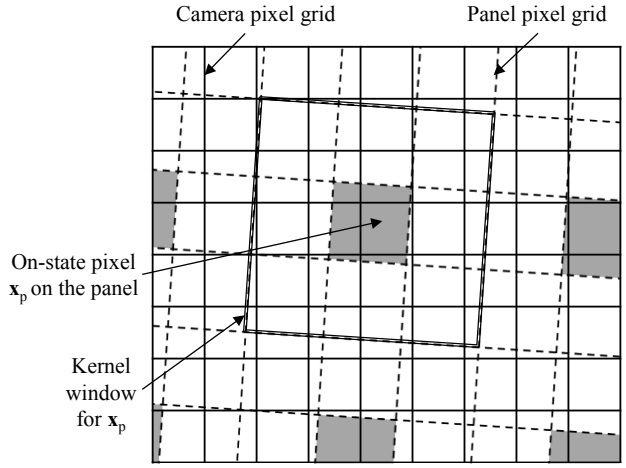

Fig. 4. Non-overlapping kernel window for panel pixel $\mathbf{x}_{\mathrm{p}}$ of on-state

To perform the measurement, we first obtain the point spread function (PSF) of the image acquisition system. Based on the PSF, we determine the minimum interval m between measuring pixels so that their responses may not interfere with each other. We then define a dot pattern image by applying a nonzero uniform gray-level only for evenly spaced dots (or panel pixels) with an interval of m while applying zero value for the others. Figure 3 shows an example of dot pattern images for $m = 3$, in which evenly spaced dots S^1 are on-state. To measure the intensities of the whole panel pixels, we need to acquire m^2 or nine dot pattern images with shifts.

For a pixel $\mathbf{x}_{\mathrm{p}}$ of on-state, the corresponding intensity can be determined via a weighted summation of intensities of captured camera pixels near the transformed pixel position $T(\mathbf{x}_{\mathrm{p}})$. In the panel coordinates, an appropriate window size, not invading the regions of neighboring on-state pixels, is m by m with the center of $\mathbf{x}_{\mathrm{p}}$. The positions of four corner points of this window are transformed into the camera coordinates by T, respectively. The kernel window of $\mathbf{x}_{\mathrm{p}}$ on the camera pixel grid is then defined as a tetragonal region enclosed by these four points, as shown in Figure 4.

The panel pixel intensity is obtained as

$$G_I(\mathbf{x}_{\mathrm{p}}) = \sum_{\mathbf{x}_{\mathrm{c}}} w_{\mathbf{x}_{\mathrm{p}}}(\mathbf{x}_{\mathrm{c}}) C_I^k(\mathbf{x}_{\mathrm{c}}) \quad \text{for } \mathbf{x}_{\mathrm{p}} \in S^k,\ k = 1, \ldots, m^2, \quad (6)$$

where $G_I(\mathbf{x}_{\mathrm{p}})$ denotes the estimated intensity of $\mathbf{x}_{\mathrm{p}}$ for input gray-level I, $\mathbf{x}_{\mathrm{c}}$ denote camera pixel positions within the kernel window, $w_{\mathbf{x}_{\mathrm{p}}}(\mathbf{x}_{\mathrm{c}})$ denote camera pixel weights, and C_I^k is a captured image of the k-th dot pattern image with an intensity of I, respectively.

2.3. Gamma curve determination

The gamma curve can be described with $G_I(\mathbf{x}_{\mathrm{p}})$ as

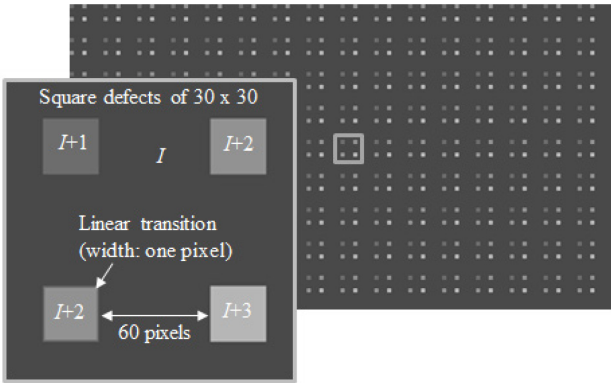

Fig. 5. Simulated defects on the panel

$$g_{\mathbf{x}_p}(I) = G_I(\mathbf{x}_p)\,. \tag{7}$$

Since G_I is measured only for sampled input gray-levels, however, continuous gamma curves can be determined via the interpolation between samples using the piecewise cubic Hermite interpolating polynomial (PCHIP). The curve is thereby smooth while it has no overshoot and less oscillation compared with spline interpolation, even when the data include some noise.

3. EXPERIMENT

In the experiment, we used a 40 inch UHD LCD panel with a 4K (3840 x 2160) resolution and an industrial monochrome camera VN-29MC with a resolution of 6476 x 4384. The camera provides 12-bit uncompressed images as the output. Apo-Componon 4.0/45 lens was mounted to the camera, whose f-number is 4.0. All experiments were conducted in a dark room.

Sampled gray-levels for the measurement were chosen as 0 (black), 16, 24, 32, 64, 96, 120, 160, 192, 224, and 255 (full-white). Exposure time is set to 2100 msec for the gray-levels from 0 to 64, and 300 msec for the gray-levels from 64 to 255, respectively. For an input gray-level of 64, the measurements were performed twice with two exposure times to determine a scaling factor between two measurements. We can thereby use two sets of measurements of different exposure times seamlessly for gamma curve estimation.

In order to verify the performance of our system based on the proposed methods, we simulated defects on a panel by slightly changing the gray-levels of repeated small squares from the original gray-level of *I*, as shown in Figure 5. The square defects were made brighter than normal background pixels as much as 1 to 3 gray-levels, and their edges were made sharp with zero- or one-pixel transition, so as to examine whether the proposed method could identify the relative luminance differences and the degree of edge sharpness.

3.1. Mapping function estimation

To estimate the mapping function *T*, we first determined corner points $\hat{\mathbf{c}}_c^i$ in the camera coordinates via the proposed two-step process described in Section 2.1.2. Since $T^{-1}(\hat{\mathbf{c}}_c^i)$ are supposed to be the same as the corner positions $\mathbf{c}_p^i$ in the panel coordinates if *T* is correct, Euclidean distances between pairs of corners $d(\mathbf{c}_p^i, \hat{T}^{-1}(\hat{\mathbf{c}}_c^i))$ can be considered mapping error. Hence, *T* is estimated as $\hat{T}$ by minimizing the mapping error. As the result, the average value of $d(\mathbf{c}_p^i, \hat{T}^{-1}(\hat{\mathbf{c}}_c^i))$ was determined as 0.0922 panel pixel with its maximum value of 0.2973 panel pixel, which roughly corresponds to the width of a sub-pixel.

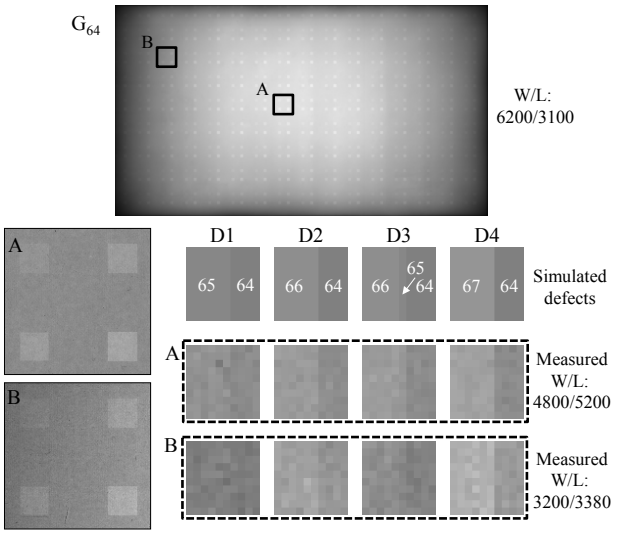

Fig. 6. A panel intensity image acquired from a uniform gray-level of 64 with simulated defects and its magnified images. An exposure time of 2100ms is used.

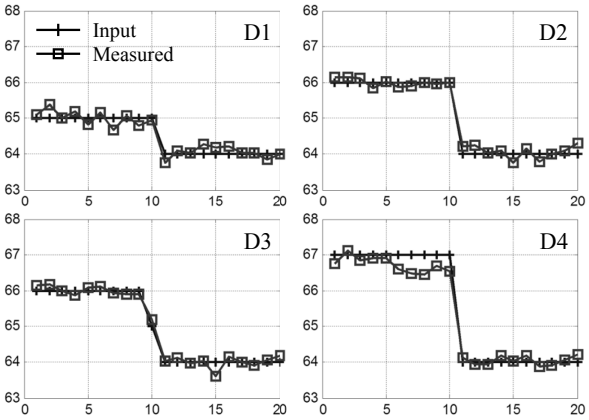

Fig. 7. Vertically averaged and normalized profiles across the defect boundaries illustrated in Figure 6.

3.2. Panel intensity image measurement

Figure 6 shows an example of measured panel intensity images, which is obtained for a gray-level of 64 with an exposure time of 2100 msec. This image is composed of panel pixel intensities that are measured using nine different dot pattern images with the same gray-level. We can easily note in the figure that the intensities of simulated defects are well observed in the measured image even

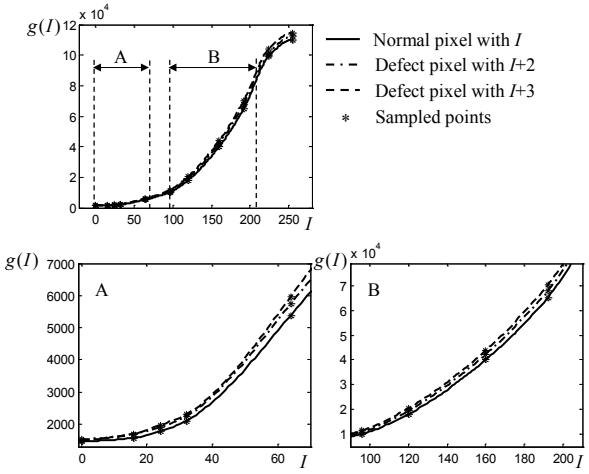

Fig. 8. Determined gamma curves for a normal pixel and two simulated defect pixels

though the intensity difference from the normal area is very small. We can also notice that edges of the defects are well observed without any degradation of sharpness. Figure 7 shows the profiles that are vertically averaged along the defect boundary and normalized, to demonstrate the vertical edge sharpness with reduced camera noise. It is note that the difference of edge transition of 1 pixel width can be easily distinct in the measurement.

3.3. Gamma curve determination

To determine gamma curves, we first determine twelve panel intensity images. Using them, we obtain gamma curves for every panel pixel via the interpolation based on PCHIP. Here, the number of curves is the same as the number of pixels, or eight mega. Figure 8 shows the determined gamma curves at three pixels arbitrarily chosen from normal and defect areas. We can note in the graphs that gamma curves are well estimated and small difference of 2 or 3 gray-level can be easily recognized in the curves.

4. CONCLUSION

In this paper, we propose an automated system to obtain gamma curves of each individual panel pixel on a high-resolution FPD. In this system, a mapping function is estimated between the panel coordinates and the camera coordinates via feature-based registration of a checkerboard pattern image. By transforming camera captured images to the panel coordinates using the mapping function, the system measures individual panel pixel intensity values without any interference from other pixels, and finally determines their gamma curves. By using the proposed system, a mapping function was obtained with the registration error less than 0.3 panel pixel, and thereby defects of 1 to 2 gray-level brightness difference were well determined with pixel accuracy.

5. ACKNOWLEDGEMENT

This work was supported by a grant from Samsung Display Co. Ltd., Korea.

REFERENCES

[1] J.-H. Kim, S. Ahn, J. W. Jeon, and J.-E. Byun, “A high-speed high-resolution vision system for the inspection of TFT LCD,” in *Proc. of IEEE International Symposium on Industrial Electronics*, Pusan, Korea, 2001, pp. 101–105.

[2] L.-C. Chen and C.-C. Kuo, “Automatic TFT-LCD mura defect inspection using discrete cosine transform-based background filtering and ‘just noticeable difference’ quantification strategies,” *Measurement Science and Technology*, vol. 19, no. 1, p. 5501, 2008.

[3] L.-F. Chen, C.-T. Su, and M.-H. Chen, “A neural-network approach for defect recognition in TFT-LCD photolithography process,” *IEEE Transactions on Electronics Packaging Manufacturing*, vol. 32, no. 1, pp. 1-8, Jan. 2009.

[4] R. S. Lu, Y. Q. Shi, Q. Li, and Q. P. Yu, “AOI techniques for surface defect inspection,” *Applied mechanics and Materials*, vol. 36, pp. 297-302, 2010.

[5] K.-C. Fan, S.-H. Chen, J.-Y. Chen, and W.-B. Liao, “Development of auto defect classification system on porosity powder metallurgy products,” *NDT & E International*, vol. 43, no. 6, pp. 451-460, 2010.

[6] D. C. Brown, “Decentering distortion of lenses,” *Photometric Engineering*, vol. 32, no. 3, pp. 444–462. May 1966.

[7] W. Förstner and E. Gülch, “A Fast operator for detection and precise location of distinct points, corners and centres of circular features,” in *Proc. ISPRS Intercommission Conference on Fast Processing of Photogrammetric Data*, pp. 281-305, 1987.

[8] T. Lindeberg, “Feature detection with automatic scale selection,” *International Journal of Computer Vision*, vol. 30, no. 2, pp. 79-116, 1998.

[9] K. Levenberg, "A method for the solution of certain problems in least-squares," *Quarterly Applied Math.*, vol. 2, pp. 164–168, 1944.

[10] D. Marquardt, "An algorithm for least-squares estimation of nonlinear parameters," *SIAM Journal Applied Math.*, vol. 11, pp. 431–441, 1963.

[11] J. J. Moré, "The Levenberg-Marquardt algorithm: Implementation and theory," *Numerical Analysis*, G. A. Watson, *Lecture Notes in Mathematics*, vol. 630, Springer Verlag, pp. 105–116, 1977.